

Entanglement-Assisted Quantum Chiral Spectroscopy

Chong Ye, Yifan Sun, and Xiangdong Zhang*

Key Laboratory of advanced optoelectronic quantum architecture and measurements of Ministry of Education, Beijing Key Laboratory of Nanophotonics & Ultrafine Optoelectronic Systems, School of Physics, Beijing Institute of Technology, 100081, Beijing, China

E-mail: zhangxd@bit.edu.cn

Abstract

The most important problem of spectroscopic chiral analysis is the inherently weak chiral signals are easily overwhelmed by the environment noises. Enormous efforts had been spent to overcome this problem by enhancing the symmetry break in the light-molecule interactions or reducing the environment noises. Here, we propose an alternative way to solve this problem by using frequency-entangled photons as probe signals and detecting them in coincidence, i.e., using quantum chiral spectroscopy. For this purpose, we develop the theory of entanglement-assisted quantum chiral spectroscopy. Our results show that the signals of left- and right-handed molecules in the quantum spectrum are always distinguishable by suitably configuring the entangled probe photons. In construct, the classical spectrum of the two enantiomers become indistinguishable when the symmetry break in the interactions is overwhelmed by the environment noises. This offers our quantum chiral spectroscopy a great advantage over all classical chiral spectroscopy. Our work opens up an exciting area that exploring profound advantages of quantum spectroscopy in chiral analysis.

Introduction

Chiral molecules cannot be superimposed with their mirror images by rotations and translations. Such stereo-isomers are called enantiomers. As with our hands, the two enantiomers can be termed by left-handed and right-handed molecules, respectively. The enantiomers of opposite chirality (handedness) play dramatically different roles in chemistry, biotechnologies, and pharmaceuticals.¹ Because the two enantiomers share almost all of their physical properties, identifying them is challenging and of great importance to the above and other relevant research areas.^{2,3}

In the passing years, spectroscopy methods of chiral analysis are developed to distinguish molecular chirality. The main idea of the methods is to induce the symmetry break in the interactions between light and two enantiomers so that the chiral difference can be mapped to the optical degrees of freedom and detected spectroscopically. By far, well established spectroscopy methods of chiral analysis include (vibrational⁴ and photoelectron⁵) circular dichroism,⁶ optical rotary dispersion,⁷ Raman optical activity,⁸ and recent three-wave mixing spectroscopy.⁹

However, the molecular size is typically smaller than the wavelengths of the applied electromagnetic fields, leading to inherently weak chiral signals. Such weak chiral signals are easily overwhelmed by the environment noises, which affect the chiral analysis in the process of light-molecule interactions and the detection process. In the first process, the symmetry break in the interactions is suppressed by the environment noises, making it difficult to map the chiral difference to optical degrees of freedom. In the second process, the environment noises make it hard to detect the chiral signals. In order to solve this problem, enormous efforts had been made to reduce the environment noises by using buffer-gas cooling,^{10,11} and direct laser cooling.^{12,13} Alternatively, advancements toward enhanced the symmetry break in light-molecule interactions have been widely explored, such as using plasmonic nanostructures,¹⁴ chiral surface,¹⁵ and twisted light with optical orbital angular momentum.¹⁶

In this Letter, we propose a quantum chiral spectroscopy to solve such a problem by using a more ingenious detecting scheme. To this end, we develop the theory of using frequency-entangled photons as probe signals and detecting them in coincidence. Attributing to the nonclassical bandwidth of the frequency-entangled photons,^{17–19} the chiral difference can be enhanced in the coincidence signals. Our results show that the signals of left- and right-handed molecules in the coincidence spectrum are always distinguishable by suitably choosing the frequency-entangled two-photon pairs. In contrast, the classical spectrum left- and right-handed molecules will become indistinguishable in the strong dissipation region, where the symmetry break in the interactions is overwhelmed by the environment noises. This offers our quantum chiral spectroscopy a great advantage over all classical chiral spectroscopes.

Model

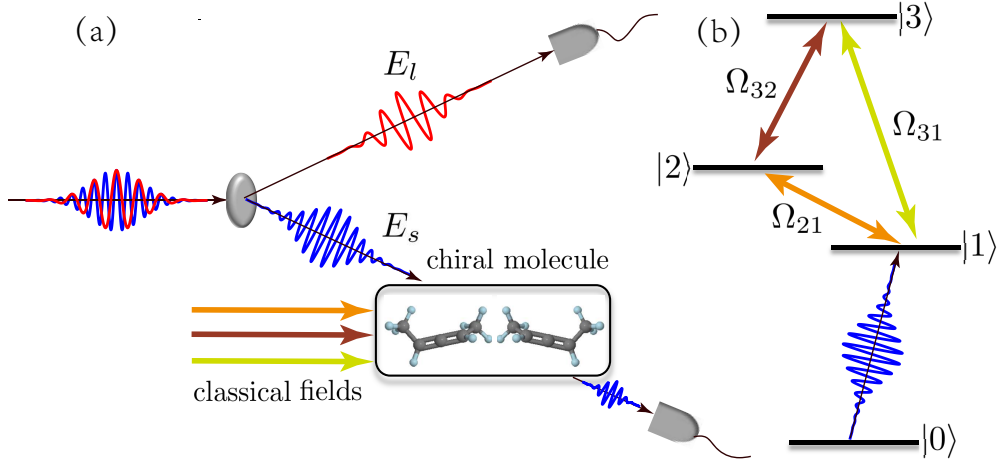


Figure 1: (a) Proposed setup for chiral analysis: Three classical fields are offered to control the chiral molecule. E_s and E_l are frequency-entangled. While E_s interacts with the chiral molecule, E_l propagates freely. The two photons are detected in coincidence. (b) The level scheme of our working system without regard to its chirality. The molecular chirality is reflected in the coupling strengths Ω_{ij} .

Our theoretical model is shown in Fig. 1 (a), where a chiral molecule couples with three narrow-band classical control fields and the signal photon of an incident broad-band entangled two-photon pair through the electric dipole interactions. A detector is used to collect

the transmitted signal photon. The idle photon will not interact with the chiral molecule and serves as a reference for the two-photon counting. We use a four-level model with a cyclic three-level configuration as shown in Fig. 1 (b) to describe our working system. The three excited states $|1\rangle$, $|2\rangle$, and $|3\rangle$ are coupled to each other in a cyclic three-level configuration through the three classical control fields. The ground state $|0\rangle$ is coupled to the excited state $|1\rangle$ through the signal photon.

The energies of molecular states $|j\rangle$ are $\hbar\omega_j$. The frequencies of the three narrow-band control fields are ν_{ij} ($i > j = 1, 2, 3$). The corresponding coupling strengths are Ω_{ij} . For simplicity, the system is set to work under the three-photon resonance condition $\nu_{31} = \nu_{21} + \nu_{32}$. For the broad-band signal and idle photons in our setup, we assume the paraxial and long wave approximations such that they can be simplified to be one-dimensional,^{17,19} respectively.

In the rotating-wave approximation, the Hamiltonian of the four-level model at $r = 0$ without regard to the molecular chirality is ($\hbar = 1$)

$$H = \sum_{j=0}^3 \omega_j \sigma_{jj} + \sum_{i>j=1}^3 (\Omega_{ij} \sigma_{ij} e^{-i\nu_{ij}t} + \text{H.c.}) + \sum_{k_s} [\omega_s a_{k_s}^\dagger a_{k_s} + (g_{k_s} a_{k_s} \sigma_{10} + \text{H.c.})] + \sum_{k_l} \omega_l a_{k_l}^\dagger a_{k_l}. \quad (1)$$

Here, we have defined $\sigma_{ij} \equiv |i\rangle\langle j|$ with $i, j = 0, 1, 2, 3$. $a_{k_s}^\dagger$ and $a_{k_l}^\dagger$ are the creation operators for the signal and idle photons with energies $\hbar\omega_s$ and $\hbar\omega_l$. The coupling strength attributing to the signal photon is $g_{k_s} = \mu\sqrt{\omega_s/(2\varepsilon_0 L)}$. Here, μ , L , and ε_0 are the transition electric dipole, the quantized volume, and the dielectric constant in the vacuum, respectively.

The chirality of our working system can survive in the electric dipole approximation. It is reflected by the three electric dipole transition moments of the cyclic three-level configuration. While their magnitudes are the same for the two enantiomers, the sign of their product is distinct for each enantiomer.^{20,21} This property plays the essential role in chiral analysis^{9,22,23} and a more ambitious issue named enantio-purification.²⁴⁻³⁰ In our four-level

model, this property is revealed by the sign of the coupling strengths Ω_{ij} . Without loss of generality, we can choose

$$\Omega_{31}^R = -\Omega_{31}^L, \quad \Omega_{21}^R = \Omega_{21}^L, \quad \Omega_{32}^R = \Omega_{32}^L. \quad (2)$$

Here, the subscripts “ $Q = L, R$ ” are used to denote the molecular chirality.

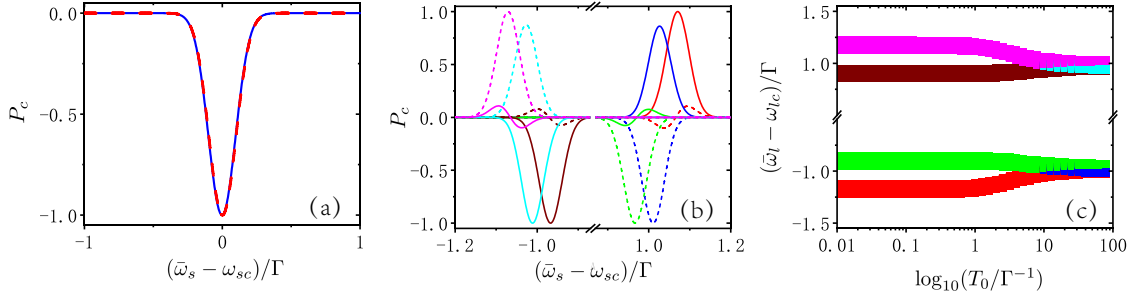


Figure 2: Classical (a) vs Quantum (b) chiral spectroscopy of left-handed (solid line) and right-handed (dashed line) molecules in strong dissipation region. In quantum chiral spectroscopy, we give six cases (distinguished by colors) corresponding to different $\bar{\omega}_l$. The spectrum of the two enantiomers have different spectral-line shapes or signs. (c) The working regimes (colored regimes) of our entanglement-assisted quantum chiral spectroscopy in the $(T_0 - \bar{\omega}_l)$ plane. Each regime in (c) corresponds to one of the six cases in (b).

Frequency-resolved chiral coincidence spectrum

In our setup, the chiral signals are collected by two-photon counting and given by coincidence probabilities in the standard Glauber’s approach.³¹ We are interested in the coincidence probabilities of detecting a single photon at r_s and a single idle photon at r_l is detected. We assume that the sensitive function of the two detectors are $\mathcal{S}\delta(\bar{\omega}_s - \omega_s)$ and $\mathcal{S}\delta(\bar{\omega}_l - \omega_l)$ with sensitive frequencies $\bar{\omega}_s$ and $\bar{\omega}_l$. Then, by fixing the sensitive frequency of one detector and scanning that of the other, we can obtain the frequency-resolved spectrum of the coincidence probability, i.e., the frequency-resolved coincidence spectrum.

In the standard Glauber’s approach,³¹ the coincidence probabilities can be achieved with the help of the system’s evolution operators, which can be obtained by using the following

procedure (see more details in Section 1 of Supplement). We treat the photon-molecule coupling $\sum_{k_s} (g_{k_s} a_{k_s} \sigma_{10} + \text{H.c.})$ as a perturbation. The remaining terms can be diagonalized in the interaction picture as $\mathcal{H}^{(0)} = \sum_{i=1}^3 \lambda_i^Q |\lambda_i^Q\rangle \langle \lambda_i^Q| + \sum_{k_s} \Delta_{k_s} a_{k_s}^\dagger a_{k_s} + \sum_{k_l} \omega_l a_{k_l}^\dagger a_{k_l}$ with $\Delta_{k_s} \equiv \omega_s - (\omega_1 - \omega_0)$. Using Dyson series, we give the evolution operators of the system and the coincidence spectrum. The coincidence spectrum are composed of two parts. One is the background, which describes the frequency-resolved coincidence probabilities without the chiral molecule. The other is the frequency-resolved transmission spectrum,¹⁸ which is the change of the frequency-resolved coincidence probabilities due to the appearance of the chiral molecule.

Since λ_i^Q are chirality-dependent, the transmission spectrum are different for the two enantiomers. Specifically, for the system initially prepared in

$$|\Psi(0)\rangle = |0\rangle \otimes \sum_{k_s, k_l} \psi(k_s, k_l) a_{k_s}^\dagger a_{k_l}^\dagger |vac\rangle \quad (3)$$

with the vacuum state of the photon field $|vac\rangle$, the transmission spectrum are (see more details in Section 2 of Supplement)

$$P_c^Q(\bar{\omega}_s, \bar{\omega}_l) = -\frac{\mathcal{S}^2 L^3}{8\pi^4} \varepsilon_{k_l}^2 \varepsilon_{k_s}^2 \sum_{i=1}^3 \sum_{k_s''} |\eta_{1\lambda_i^Q}|^2 \Re \left[\frac{g_{\bar{k}_s}^* g_{k_s''} \psi^*(\bar{k}_s, \bar{k}_l) \psi(k_s'', \bar{k}_l)}{(\lambda_i^Q - \Delta_{\bar{k}_s} + i\Gamma)(\lambda_i^Q - \Delta_{k_s''} + i\Gamma)} \right] \quad (4)$$

with $\varepsilon_{k_s} = \sqrt{\omega_s/(2\varepsilon_0 L)}$, $\varepsilon_{k_l} = \sqrt{\omega_l/(2\varepsilon_0 L)}$, $\bar{k}_s = \bar{\omega}_s/c$, $\bar{k}_l = \bar{\omega}_l/c$, and $\eta_{1\lambda_i^Q} = \langle 1|\lambda_i^Q\rangle$. c is the speed of light in vacuum. The environment noises will affect the process of the light-molecule interactions, which give rise to the dissipation of molecules. In order to describe the effect of dissipation, we have introduced Γ in Eq. (4).

Entanglement-enhanced chiral analysis

In general, the chirality dependency in the transmission spectrum is independent of whether the two photons are entangled or not. However, in the classical chiral spectroscopy, where

the two uncorrelated photons are used, the spectral broadening caused by dissipation will reduce the chirality dependency and eventually make the transmission spectrum of the two enantiomers become indistinguishable. In contrast, in quantum chiral spectroscopy, where frequency-entangled photons are used as probe signals, the signal can be filtered and thus the chirality dependency in the transmission spectrum can be enhanced.

In order to demonstrate such an advantage of quantum chiral spectroscopy, we set the chiral molecule in the strong dissipation region by choosing the coupling strengths for the two enantiomers as $\Omega_{31}^R = -\Omega_{31}^L = 0.1\Gamma$, $\Omega_{21}^R = \Omega_{21}^L = 0.1\Gamma$, and $\Omega_{32}^R = \Omega_{32}^L = 0.1\Gamma$. The three classical control fields are coupled with their corresponding transitions on resonance with $\Delta_{21} = \Delta_{31} = 0$. Under these parameters, the classical transmission spectrum of the two enantiomers are indistinguishable as shown in Fig. 2(a). For calculations, we have used uncorrelated two-photon pairs with center frequencies ω_{sc} and ω_{lc} by choosing $\psi(k_s, k_l) \propto \exp\{-[(\omega_s - \omega_{sc})^2 + (\omega_l - \omega_{lc})^2]/(2\sigma^2)\}$ with width $\sigma = \Gamma$.

For the case of frequency entangled two-photon pairs, we use¹⁸

$$\psi(k_s, k_l) \propto A_p(k_s, k_l) \exp(-\kappa^2). \quad (5)$$

Such two-photon pairs can be generated in nonlinear crystals due to the downconversion process.¹⁹ The envelope $A_p(k_s, k_l)$ is given by the pumped pulse. Here, we use a Gaussian envelop with $A_p(k_s, k_l) = \exp[-(\omega_l + \omega_s - \omega_p)^2/(2\sigma_p^2)]$ with the center frequency ω_p and the width σ_p . The phase-mismatching function $\exp(-\kappa^2)$ appearances due to the propagation of photons in the crystals. For entangled two-photon pairs generated in type-II nonlinear crystals, we approximately have¹⁷⁻¹⁹

$$\kappa = (\omega_s - \omega_{sc})\frac{T_s}{2} + (\omega_l - \omega_{lc})\frac{T_l}{2} \quad (6)$$

with the center frequencies of the two photons ω_{sc} and ω_{lc} . T_s and T_l are the maximal time delays of the two photons propagating in the crystals with respect to the pumped pulse.

In Fig. 2(b), we show the transmission spectrum of the two enantiomers in the strong dissipation region by using entangled two-photon pair with $\sigma_p = \Gamma$, $T_s = 2.4 \times 10^1 \Gamma^{-1}$, and $T_l = 2.5 \times 10^1 \Gamma^{-1}$. By tuning $\bar{\omega}_l$, the transmission spectrum of the two enantiomers with respect to $\bar{\omega}_s$ can have different spectral-line shapes or signs. Here, we have illustrated six cases distinguished by color. Comparing these results with that in Fig. 2(a), we can conclude that the chiral analysis using frequency entangled two-photon pairs is overwhelming advantage over that using uncorrelated ones in the strong dissipation region. The advantage is due to the appearance of frequency entanglement. In this sense, we have demonstrated an entanglement-assisted quantum chiral spectroscopy in the strong dissipation region.

In addition to $\bar{\omega}_l$, T_s and T_l are other two additional tunable parameters in quantum spectroscopy comparing with the classical spectroscopy. It is natural to explore the working regimes of our entanglement-assisted quantum chiral spectroscopy with respect to $\bar{\omega}_l$, T_s and T_l . For simplicity, we have used $T_s = 2.4T_0$ and $T_l = 2.5T_0$. The results are shown in Fig 2(c). Our entanglement-assisted quantum chiral spectroscopy works in the colored regimes of the $(T_0 - \bar{\omega}_l)$ plane. Each regime in Fig. 2(c) corresponds to one of the six cases in Fig. 2(b) and is marked by the same color. These results indicate that the entanglement-assisted quantum chiral spectroscopy is robust against the variations of the entangled two-photon pairs and the detector.

Physical role of correlation

The frequency correlation between the two photons plays an important role in our entanglement-assisted quantum chiral spectroscopy. In order to illustrate this explicitly, we consider a photon pair with a zero-bandwidth negative energy correlation, given by¹⁹

$$\psi(k_s, k_l) = \phi_s(k_s)\delta(\omega_l + \omega_s - \omega_p). \quad (7)$$

The delta function $\delta(\omega_l + \omega_s - \omega_p)$ indicates the energy conservation of two photons. Moreover, we choose $\Delta_{12} = \Delta_{13} \gg \{|\Omega_{12}|, |\Omega_{13}|\}$. In this case, to the second order, the dressed state $|\lambda_1^Q\rangle \simeq |1\rangle$,²⁴ i.e., $\eta_{1\lambda_2^Q} \simeq 0$ and $\eta_{1\lambda_3^Q} \simeq 0$. The transmission spectrum can be greatly simplified as

$$P_c^Q(\bar{\omega}_s, \bar{\omega}_l) = -\frac{\mathcal{S}^2 L^4}{16\pi^4} \varepsilon_{\bar{k}_l}^2 \varepsilon_{\bar{k}_s}^2 \delta(\bar{\omega}_l + \bar{\omega}_s - \omega_p) |\eta_{1\lambda_1^Q}|^2 \Re \left[\frac{g_{\bar{k}_s} g_{\bar{k}_{pl}} \phi_s^*(\bar{k}_s) \phi_s(\bar{k}_{pl})}{(\lambda_1^Q - \Delta_{\bar{k}_s} + i\Gamma)(\lambda_1^Q - \Delta_{\bar{k}_{pl}} + i\Gamma)} \right] \quad (8)$$

with $\bar{k}_{pl} \equiv k_p - \bar{k}_l$. Due to the delta function in $\psi(k_s'', \bar{k}_l)$, only the term of $k_s'' = k_p - \bar{k}_l$ with $k_p = \omega_p/c$ is nonzero and will contribute to the summation over k_s'' in Eq. (4), i.e., the correlation filters our signals.

The entanglement-assisted quantum chiral spectroscopy is also robust against the variation of dissipation. For a fixed $\bar{\omega}_l$, P_c is nonzero at $\bar{\omega}_s = \omega_p - \bar{\omega}_l$, i.e., $\bar{k}_s = \bar{k}_{pl}$. The sign of P_c^Q is determined by the sign of $[(\lambda_1^Q - \Delta_{\bar{k}_{pl}})^2 - \Gamma^2]$. Since $\lambda_1^L \neq \lambda_1^R$,³² P_c^Q have different signs for the two enantiomers when $\Delta_{\bar{k}_{pl}} = \omega_p - \bar{\omega}_l - (\omega_1 - \omega_0)$ is in the range between $(\Gamma - \lambda_1^L)$ and $(\Gamma - \lambda_1^R)$. Since the photon pair with a zero-bandwidth negative energy correlation can be approximately achieved by adjusting the width of the pumped pulse and the delay times,¹⁹ the transmission spectrum of the two enantiomers are always distinguishable in the quantum chiral spectroscopy by suitable choosing the entangled photons.

Discussions and Conclusions

In summary, we have developed the theory of entanglement-assisted quantum chiral spectroscopy to detect the molecular chirality. It offers an alternative way for suppressing the effect of environment noises on chiral analysis. Using a theoretical model, we have demonstrated that attributing to the nonclassical bandwidth of the frequency-entangled photons, the chiral difference can be enhanced in the coincidence signals. It can be applied to distinguish the molecular chirality in the strong dissipation region, where the classical chiral spectroscopy based on uncorrelated light loses efficiency due to the dissipation-induced spec-

tral broadening.

As an experimentally accessible approach, frequency-entangled photons can be produced by spontaneous parametric down conversion. The apparatuses for generating the required entangled photons in our discussions are actually available. For example, when the transition $|0\rangle \leftrightarrow |1\rangle$ is between vibrational levels, the signal photon is in the optical domain, which has been broadly investigated.³³ Also, the cyclic three-level configuration can be realized in the optical domain,²⁵ which means the whole procedure is workable in such a frequency domain.

Quantum spectroscopy that using frequency-entangled photons as probe signals is gaining attentions due to unique features of frequency-entangled photons, such as quantum fluctuations,³⁴ linear scaling behaviors,³⁵ and nonclassical bandwidth.¹⁷⁻¹⁹ We for the first time introduce it to chiral analysis and demonstrate the advantage of using frequency-entangled photons as probe signals due to their nonclassical bandwidth. Despite this, quantum spectroscopy had been demonstrated to achieve technical benefits, such as probing of the enormous range of wavelengths using visible photons,^{36,37} to offer the possibility of cancelling uncorrelated background optical noises, and noises of the detectors,³⁸ and to achieve a provable quantum advantage over all schemes using classical sources.³⁹ Our work opens up an exciting area that exploring the profound advantages of quantum spectroscopy in chiral analysis.

Acknowledgement

The authors thank the support by National Natural Science Foundation of China (No. 91850205), National Science Foundation for Young Scientists of China (No.11904022), and Beijing Institute of Technology Research Fund Program for Young Scholars.

Supporting Information Available

Derivation of frequency-resolved chiral coincidence signals.

References

- (1) Latscha, H. P.; Kazmaier, U.; Klein, H. A. *Chemie für Biologen*; Springer, 2008; Vol. 7.
- (2) Quack, M.; Stohner, J.; Willeke, M. High-resolution spectroscopic studies and theory of parity violation in chiral molecules. *Annu. Rev. Phys. Chem.* **2008**, *59*, 741–769.
- (3) Saito, Y.; Hyuga, H. Colloquium: Homochirality: Symmetry breaking in systems driven far from equilibrium. *Reviews of Modern Physics* **2013**, *85*, 603.
- (4) Nafie, L. A. *Vibrational optical activity: principles and applications*; John Wiley & Sons, 2011.
- (5) Beaulieu, S.; Comby, A.; Descamps, D.; Fabre, B.; Garcia, G.; Généaux, R.; Harvey, A.; Légaré, F.; Mašín, Z.; Nahon, L., et al. Photoexcitation circular dichroism in chiral molecules. *Nature Physics* **2018**, *14*, 484–489.
- (6) Berova, N.; Nakanishi, K.; Woody, R. W. *Circular dichroism: principles and applications*; John Wiley & Sons, 2000.
- (7) Berova, N.; Polavarapu, P. L.; Nakanishi, K.; Woody, R. W. *Comprehensive Chiroptical Spectroscopy: Instrumentation, Methodologies, and Theoretical Simulations*; John Wiley & Sons, 2011; Vol. 1.
- (8) Barron, L. D. *Molecular light scattering and optical activity*; Cambridge University Press, 2009.
- (9) Patterson, D.; Schnell, M.; Doyle, J. M. Enantiomer-specific detection of chiral molecules via microwave spectroscopy. *Nature* **2013**, *497*, 475–477.
- (10) Hutzler, N. R.; Lu, H.-I.; Doyle, J. M. The buffer gas beam: An intense, cold, and slow source for atoms and molecules. *Chemical Reviews* **2012**, *112*, 4803–4827.

- (11) Patterson, D.; Doyle, J. M. Cooling molecules in a cell for FTMW spectroscopy. *Molecular Physics* **2012**, *110*, 1757–1766.
- (12) Mitra, D.; Vilas, N. B.; Hallas, C.; Anderegg, L.; Augenbraun, B. L.; Baum, L.; Miller, C.; Raval, S.; Doyle, J. M. Direct laser cooling of a symmetric top molecule. *Science* **2020**, *369*, 1366–1369.
- (13) Augenbraun, B. L.; Doyle, J. M.; Zelevinsky, T.; Kozyryev, I. Molecular asymmetry and optical cycling: laser cooling asymmetric top molecules. *Physical Review X* **2020**, *10*, 031022.
- (14) Wu, T.; Zhang, W.; Zhang, H.; Hou, S.; Chen, G.; Liu, R.; Lu, C.; Li, J.; Wang, R.; Duan, P., et al. Vector exceptional points with strong superchiral fields. *Physical Review Letters* **2020**, *124*, 083901.
- (15) Barcellona, P.; Safari, H.; Salam, A.; Buhmann, S. Y. Enhanced chiral discriminatory van der Waals interactions mediated by chiral surfaces. *Physical Review Letters* **2017**, *118*, 193401.
- (16) Forbes, K. A. Raman optical activity using twisted photons. *Physical Review Letters* **2019**, *122*, 103201.
- (17) Dorfman, K. E.; Schlawin, F.; Mukamel, S. Stimulated Raman Spectroscopy with Entangled Light: Enhanced Resolution and Pathway Selection. *the Journal of Physical Chemistry Letters* **2014**, *5*, 2843–2849.
- (18) Schlawin, F.; Dorfman, K. E.; Mukamel, S. Pump-probe spectroscopy using quantum light with two-photon coincidence detection. *Phys. Rev. A* **2016**, *93*, 023807.
- (19) Dorfman, K. E.; Schlawin, F.; Mukamel, S. Nonlinear optical signals and spectroscopy with quantum light. *Rev. Mod. Phys.* **2016**, *88*, 045008.

- (20) Král, P.; Shapiro, M. Cyclic Population Transfer in Quantum Systems with Broken Symmetry. *Phys. Rev. Lett.* **2001**, *87*, 183002.
- (21) Ye, C.; Zhang, Q.; Li, Y. Real single-loop cyclic three-level configuration of chiral molecules. *Physical Review A* **2018**, *98*, 063401.
- (22) Ye, C.; Zhang, Q.; Chen, Y.-Y.; Li, Y. Determination of enantiomeric excess with chirality-dependent AC Stark effects in cyclic three-level models. *Physical Review A* **2019**, *100*, 033411.
- (23) Wu, J.-L.; Wang, Y.; Su, S.-L.; Xia, Y.; Jiang, Y.; Song, J. Discrimination of enantiomers through quantum interference and quantum Zeno effect. *Opt. Express* **2020**, *28*, 33475–33489.
- (24) Li, Y.; Bruder, C.; Sun, C. P. Generalized Stern-Gerlach Effect for Chiral Molecules. *Phys. Rev. Lett.* **2007**, *99*, 130403.
- (25) Vitanov, N. V.; Drewsen, M. Highly Efficient Detection and Separation of Chiral Molecules through Shortcuts to Adiabaticity. *Phys. Rev. Lett.* **2019**, *122*, 173202.
- (26) Ye, C.; Zhang, Q.; Chen, Y.-Y.; Li, Y. Effective two-level models for highly efficient inner-state enantioseparation based on cyclic three-level systems of chiral molecules. *Physical Review A* **2019**, *100*, 043403.
- (27) Ye, C.; Zhang, Q.; Chen, Y.-Y.; Li, Y. Fast enantioconversion of chiral mixtures based on a four-level double- Δ model. *Physical Review Research* **2020**, *2*, 033064.
- (28) Ye, C.; Liu, B.; Chen, Y.-Y.; Li, Y. Enantio-conversion of chiral mixtures via optical pumping. *Physical Review A* **2021**, *103*, 022830.
- (29) Eibenberger, S.; Doyle, J.; Patterson, D. Enantiomer-Specific State Transfer of Chiral Molecules. *Phys. Rev. Lett.* **2017**, *118*, 123002.

- (30) Pérez, C.; Steber, A. L.; Domingos, S. R.; Krin, A.; Schmitz, D.; Schnell, M. Coherent Enantiomer-Selective Population Enrichment Using Tailored Microwave Fields. *Angewandte Chemie International Edition* **2017**, *56*, 12512–12517.
- (31) Glauber, R. J. *Quantum theory of optical coherence: selected papers and lectures*; John Wiley & Sons, 2007.
- (32) Kang, Y.-H.; Shi, Z.-C.; Song, J.; Xia, Y. Effective discrimination of chiral molecules in a cavity. *Opt. Lett.* **2020**, *45*, 4952–4955.
- (33) Prabhakar, S.; Shields, T.; Dada, A. C.; Ebrahim, M.; Taylor, G. G.; Morozov, D.; Erotokritou, K.; Miki, S.; Yabuno, M.; Terai, H.; Gawith, C.; Kues, M.; Caspani, L.; Hadfield, R. H.; Clerici, M. Two-photon quantum interference and entanglement at 2.1 μm . *Science Advances* **2020**, *6*.
- (34) Kira, M.; Koch, S. W.; Smith, R. P.; Hunter, A. E.; Cundiff, S. T. Quantum spectroscopy with Schrödinger-cat states. *Nature Physics* **2011**, *7*, 799–804.
- (35) Dayan, B.; Pe’er, A.; Friesem, A. A.; Silberberg, Y. Nonlinear Interactions with an Ultrahigh Flux of Broadband Entangled Photons. *Phys. Rev. Lett.* **2005**, *94*, 043602.
- (36) Scarcelli, G.; Valencia, A.; Gompers, S.; Shih, Y. Remote spectral measurement using entangled photons. *Applied Physics Letters* **2003**, *83*, 5560–5562.
- (37) Kalashnikov, D. A.; Paterova, A. V.; Kulik, S. P.; Krivitsky, L. A. Infrared spectroscopy with visible light. *Nature Photonics* **2016**, *10*, 98–101.
- (38) Kalashnikov, D. A.; Pan, Z.; Kuznetsov, A. I.; Krivitsky, L. A. Quantum spectroscopy of plasmonic nanostructures. *Physical Review X* **2014**, *4*, 011049.
- (39) Shi, H.; Zhang, Z.; Pirandola, S.; Zhuang, Q. Entanglement-Assisted Absorption Spectroscopy. *Phys. Rev. Lett.* **2020**, *125*, 180502.

TOC Graphic

Some journals require a graphical entry for the Table of Contents. This should be laid out “print ready” so that the sizing of the text is correct.

Inside the tocentry environment, the font used is Helvetica 8 pt, as required by *Journal of the American Chemical Society*.

The surrounding frame is 9 cm by 3.5 cm, which is the maximum permitted for *Journal of the American Chemical Society* graphical table of content entries. The box will not resize if the content is too big: instead it will overflow the edge of the box.

This box and the associated title will always be printed on a separate page at the end of the document.